Isospin mixing effects in the low-energy $\bar{K}N$-$\pi\Sigma$ interaction

J. Révai[1] and N. V. Shevchenko[2,*]

[1]*Research Institute for Particle and Nuclear Physics, H-1525 Budapest, P.O.B. 49, Hungary*

[2]*Nuclear Physics Institute, 25068 Rez, Czech Republic*

(Received 31 October 2008; revised manuscript received 19 January 2009; published 3 March 2009; publisher error corrected 6 March 2009)

New strong coupled-channels $\bar{K}N$-$\pi\Sigma$ potential, reproducing all existing experimental data and suitable for using in an accurate few-body calculations, is constructed. Isospin breaking effects of direct inclusion of the Coulomb interaction and using of physical masses in calculations are investigated. The $1s$ level shift and width of kaonic hydrogen, consistent with the scattering data, was obtained and the corresponding exact strong K^-p scattering length was calculated. One- and two-pole form of $\Lambda(1405)$ resonance was considered.

DOI: 10.1103/PhysRevC.79.035202 PACS number(s): 13.75.Jz, 11.80.Gw, 21.45.−v, 36.10.Gv

I. INTRODUCTION

Kaonic atoms and, especially, the possibility of the formation of kaonic nuclear clusters has recently attracted much interest. For investigation of these systems it is necessary to know the basic $\bar{K}N$ interaction, which is strongly connected with $\pi\Sigma$ and other channels.

Different theoretical models were used for constructing the antikaon-nucleon interaction. All these models can be separated in two groups: "stand-alone" potentials having the only aim to fit two-body data and potentials to be used in future (few- or many-body) calculations.

The first group comprises potentials based on chiral Lagrangians. The method, quite popular these days, consists of constructing a potential which gives amplitudes equivalent to those derived from an effective chiral Lagrangian. Such potentials have many channels, including energetically closed near $\bar{K}N$ threshold ones. The most recent example is a model constructed in Refs. [1,2]. It is good in reproducing the antikaon-nucleon experimental data; however, due to its unwieldy the potential cannot be used in few- or many-body calculations.

However, effective potentials used in approximate few-body calculations are too simple for proper describing of all properties of the $\bar{K}N$ system. In most cases a one-channel (effective) optical potential is used. For example, the $\bar{K}N$ potential, used in Ref. [3] for calculating deeply bound kaonic nuclear states, is an energy-independent optical potential. It was constructed in such a way that it corresponds to the elastic part of a coupled-channels phenomenological $\bar{K}N$-$\pi\Sigma$-$\pi\Lambda$ potential. However, already the original coupled-channels potential is too simple. One more example is a recent work [4], where a potential for further use in a few-body calculation was derived. It is once more an effective energy-dependent optical potential by construction: it reproduces the elastic part of an effective chiral coupled-channels model.

Two-body optical potentials could be equivalent in a certain sense to the original coupled-channels ones. For separable potentials it is possible to construct exact optical potential, but even an exact optical potential properly describes only the elastic part of the whole system. Moreover, introducing such "good" effective optical potentials into $N > 2$ equations does not guarantee proper description of all inelastic effects taking place in a few- or many-body system.

The inelastic effects are especially important for the antikaon-nuclear systems, because $\bar{K}N$ interaction is strongly coupled to the $\pi\Sigma$ channel through $\Lambda(1405)$ resonance. However, the nature of the resonance is a separate question. A usual assumption is that $\Lambda(1405)$ is a resonance in $\pi\Sigma$ and a quasi-bound state in the $\bar{K}N$ channel. There is also an assumption suggested by a chiral model that the bump, which is usually understood as $\Lambda(1405)$ resonance, is an effect of two poles (see e.g. Refs. [5,6]). Some challenge to the two-pole model was put forth by the recent experiment at COSY-Jülich [7], but according to a subsequent theoretical paper [8] it seems to be possible to reproduce the experiment on the basis of the two-pole model.

Other sources of experimental data about $\bar{K}N$ interaction are also nonprecise, old, or controversial. The data on cross sections of elastic and inelastic scattering with K^-p in the initial state are rather old with quite large errors, while threshold branching ratios of K^-p scattering were measured more accurately.

Another source of knowledge about $\bar{K}N$ is the kaonic hydrogen atom. Several experiments were performed for measuring $1s$ level shift caused by the strong $\bar{K}N$ interaction. The two recent ones are KEK [9] and DEAR [10] results. The more recent DEAR value of the $1s$ level shift and width significantly differs from the older KEK result; it has smaller errors but is inconsistent with the K^-p scattering data as was shown in Refs. [1,2].

Moreover, there is a problem common for both experimental papers: they present a K^-p scattering length following from the measurements as an "experimental value." However, a_{K^-p} values in Refs. [9] and [10] were obtained using the Deser-Trueman (DT) formula [11], while in many papers (among them in Ref. [12] for several one-channel model potentials) it was shown that the approximate formula has poor accuracy, in particular for the $\bar{K}N$ interaction. There are several papers introducing different corrections to DT; these days the most popular is a formula from Ref. [13]. Undoubtedly, the corrected formula [13] has the same ad-

*Corresponding author: shevchenko@ujf.cas.cz

vantage as original DT [11] one: it is a model-independent relation between scattering length and atomic level shift and width. Its accuracy can be checked within a potential model where exact calculations are feasible.

Since the measured value is the $1s$ level shift and width (and not the K^-p scattering length) we decided to construct a phenomenological coupled-channels potential, reproducing kaonic hydrogen's level shift and width without intermediate reference to a_{K^-p}. It is clear that for reproducing the level shift of kaonic hydrogen it is necessary to include Coulomb interaction into equations directly, which breaks isospin symmetry. As far as we know, the only attempt to do the same was performed in Ref. [14]. The authors used their own method for calculating kaonic atomic state with separable chiral-based strong part of the potential and tried to reproduce DEAR data. However, the resulting potential [14] provides a too-large width Γ of the $1s$ kaonic hydrogen level in comparison with DEAR values; moreover, there are problems with reproducing $\Lambda(1405)$ resonance. The first version of our $\bar{K}N$-$\pi\Sigma$ potential reproducing the $1s$ level shift instead of the K^-p scattering length with direct inclusion of the Coulomb interaction, and the corresponding three-body $\bar{K}NN$-$\pi\Sigma N$ calculation using the obtained potential, was presented in Ref. [15].

There is one more approximation which is widely used in theoretical models, namely neglecting the mass difference in isomultiplets. However, the difference of masses between proton and neutron and K^- and $\bar{K}^0$ is a physical fact. In addition, the effect of taking the mass difference into account is especially important in the near-threshold $\bar{K}N$ region which is our main concern. Using the physical masses in the calculations is one more isospin symmetry breaking effect, taken into account in the paper.

Thus, our aim is to construct a phenomenological coupled-channels $\bar{K}N$-$\pi\Sigma$ potential, which within the limits of the possible simultaneously reproduces all experimental data: the level shift and width of kaonic hydrogen $1s$ level (KEK or DEAR values), K^-p threshold branching ratios, elastic and inelastic K^-p scattering, and $\Lambda(1405)$ resonance in one- or two-pole form. We directly include such isospin breaking effects as Coulomb interaction and using the physical masses of particles in the calculations. The corresponding T matrix should be suitable for using in an accurate few-body (for example, a three-body coupled-channels Faddeev) calculation.

II. FORMULATION OF THE PROBLEM

Our nonrelativistic Hamiltonian has the form

$$H = H^0 + V^c + V^s, \tag{1}$$

with H^0 being the kinetic energy plus the threshold energy of particle pairs, V^c and V^s denote their Coulomb and strong interaction, respectively. The transition matrix for the problem defined by this Hamiltonian can be written as

$$T_{ba} = T^c_{ba} + T^{sc}_{ba}, \tag{2}$$

where T^c_{ba} is the pure Coulomb transition matrix, while T^{sc}_{ba} is the so-called Coulomb-modified strong transition matrix, defined as

$$T^{sc}_{ba} = \langle \Phi^{c(-)}_b | V^s | \Psi^{(+)}_a \rangle. \tag{3}$$

Here $|\Phi^{c(\pm)}_b\rangle$ is a Coulomb scattering state labeled by the final-state index b, while $|\Psi^{(+)}_a\rangle$ denotes the total scattering state, corresponding to the initial state labeled a and satisfying the Lippmann-Schwinger equation

$$|\Psi^{(+)}_a\rangle = |\Phi^{c(+)}_a\rangle + G^c(E + i\varepsilon)V^s|\Psi^{(+)}_a\rangle \tag{4}$$

with the Coulomb Green's function

$$G^c(z) = (z - H^0 - V^c)^{-1}. \tag{5}$$

For a separable strong potential taken as $V^s = |g\rangle\lambda\langle g|$ the T^{sc}_{ba} matrix (3) has the form

$$T^{sc}_{ba} = \langle \Phi^{c(-)}_b | g \rangle (\lambda^{-1} - \langle g | G^c(E + i\varepsilon) | g \rangle)^{-1} \langle g | \Phi^{c(+)}_a \rangle. \tag{6}$$

For sufficiently simple form factors $|g\rangle$ the matrix elements of the Coulomb Green's function $\langle g|G^c(E + i\varepsilon)|g\rangle$ together with the overlaps $\langle g|\Phi^{c(\pm)}_a\rangle$ in Eq. (6) can be calculated analytically (see e.g. Refs. [16–18]). The poles of the total $T_{ba}(z)$ matrix in this case are determined by the equation

$$\lambda^{-1} - \langle g | G^c(z) | g \rangle = 0, \tag{7}$$

since it can be shown that the poles of the pure Coulomb T^c_{ba} matrix are canceled out from Eq. (2).

The nonrelativistic description of transitions allowing for change of particle composition is achieved by enlarging the Hilbert space by adding to it a discrete "particle composition" index. In this case the operators and wave functions become matrices and vectors with respect to this index. The details of the matrix formulation of Eqs. (3)–(7) are described in the appendix.

III. DETAILS OF THE CALCULATION AND THE INPUT

In momentum representation the strong interaction matrix (A16) can be written as:

$$V^s_{\mathbb{I}_i,\mathbb{I}_j}(k_{\mathbb{I}_i}, k_{\mathbb{I}_j}) = \delta_{I(\mathbb{I}_i),I(\mathbb{I}_j)}\, g_{\mathbb{I}_i}(k_{\mathbb{I}_i})\lambda_{\mathbb{I}_i,\mathbb{I}_j}\, g_{\mathbb{I}_j}(k_{\mathbb{I}_j}), \tag{8}$$

with $g_{\mathbb{I}_i}(k_{\mathbb{I}_i}) = \langle \vec{k}_{\mathbb{I}_i} | g_{\mathbb{I}_i} \rangle$, $\vec{k}_{\mathbb{I}_i}$ being the relative momentum of the particles in $\mathbb{I}_i$. We use the $\hbar = c = 1$ system of units, our plane waves are normalized as $\langle \vec{k} | \vec{k}' \rangle = \delta(\vec{k} - \vec{k}')$. In this case the scattering amplitude f_{ba} is connected with T_{ba} by:

$$f_{ba} = -(2\pi)^2 \sqrt{\mu_a \mu_b}\; T_{ba}, \tag{9}$$

where μ_a (μ_b) is the reduced mass of the particles in the initial (final) state.

We tried to reproduce simultaneously the following experimental data (A–D).

A. Λ(1405) resonance

Mass M_Λ and width Γ_Λ of the $\Lambda(1405)$ resonance according to the Particle Data Group [19] are:

$$M^{\rm PDG}_\Lambda = 1406.5 \pm 4.0\ {\rm MeV}, \quad \Gamma^{\rm PDG}_\Lambda = 50.0 \pm 2.0\ {\rm MeV}. \tag{10}$$

Unlike with PDG, our $\Lambda(1405)$ is not a clear $I = 0$ state but a mixture of $I = 0$ and $I = 1$ states. Having in mind existing assumptions, we used two versions of $\Lambda(1405)$'s "nature": one- and two-pole ones. For the one-pole form of $\Lambda(1405)$ we used Yamaguchi form factors:

$$g_{\mathbb{I}_i}^{1\text{pole}}(k_{\mathbb{I}_i}) = \frac{1}{(k_{\mathbb{I}_i})^2 + (\beta_{\mathbb{I}_i})^2}, \quad i = 1, \ldots, 5. \tag{11}$$

We assumed $\Lambda(1405)$ as a resonance in $\pi\Sigma$ and a quasibound state in $\bar{K}N$ channel. So, calculation of (A21) was done at physical sheet for $\bar{K}N$ and nonphysical sheet for $\pi\Sigma$ channel.

For the two-pole case we assumed that there are two resonances in the $\pi\Sigma$ channel. One of them, as before, originates from a bound state in the $\bar{K}N$ channel and the other one from a resonance in the $\pi\Sigma$ channel (with $\bar{K}N$-$\pi\Sigma$ coupling switched off). It is known that in a one-channel case a one-term separable potential with Yamaguchi form factors (11) and real strength parameters cannot describe a resonance. So to have a resonance in the uncoupled $\pi\Sigma$ channel, for the two-pole $\Lambda(1405)$ case we used $\pi\Sigma$ form factors in the following form:

$$g_{\mathbb{I}_i}^{2\text{pole}}(k_{\mathbb{I}_i}) = \frac{1}{(k_{\mathbb{I}_i})^2 + (\beta_{\mathbb{I}_i})^2} + \frac{s(\beta_{\mathbb{I}_i})^2}{\left[(k_{\mathbb{I}_i})^2 + (\beta_{\mathbb{I}_i})^2\right]^2}, \quad i = 3, 4, 5. \tag{12}$$

By this for the two-pole case we introduced one more parameter s. For the $\bar{K}N$ channel here we used Yamaguchi form factors:

$$g_{\mathbb{I}_i}^{2\text{pole}}(k_{\mathbb{I}_i}) = \frac{1}{(k_{\mathbb{I}_i})^2 + (\beta_{\mathbb{I}_i})^2}, \quad i = 1, 2. \tag{13}$$

Both poles are once more situated at physical sheet for $\bar{K}N$ and nonphysical sheet for the $\pi\Sigma$ channel.

B. Kaonic hydrogen data

The K^-p atomic $1s$ level shift ΔE_{1s} and width Γ_{1s} measured in the KEK experiment [9]

$$\Delta E_{1s}^{\text{KEK}} = -323 \pm 63 \pm 11 \text{ eV}, \quad \Gamma_{1s}^{\text{KEK}} = 407 \pm 208 \pm 100 \text{ eV} \tag{14}$$

and in the DEAR Collaboration experiment [10]

$$\Delta E_{1s}^{\text{DEAR}} = -197 \pm 37 \pm 6 \text{ eV}, \quad \Gamma_{1s}^{\text{DEAR}} = 249 \pm 111 \pm 30 \text{ eV} \tag{15}$$

differ from each other. We tried to reproduce both these values within the 1σ interval.

We stress that in our approach there is no intermediate reference to K^-p scattering length when reproducing the level shift and the width. Of course, after finding a set of potential parameters we can calculate a strong scattering length which exactly corresponds to the obtained $1s$ level shift ΔE_{1s} and width Γ_{1s}. Due to the isospin symmetry breaking, the formula for the a_{K^-p} differs from the commonly used $\frac{1}{2}(a_{\bar{K}N,I=0} + a_{\bar{K}N,I=1})$ since our T matrix has nondiagonal elements between the $I = 0$ and $I = 1$ states.

We mention here that energies of atomic (kaonic hydrogen $1s$ level) and nuclear [one- and two-pole $\Lambda(1405)$] states are obtained from the same system of equations (A21). The second remark concerns the origin of the resonances. All our resonances are poles on the corresponding sheet of the complete problem. Since our formula (A21) was obtained by solving dynamical equations, the resonances can be rightly called dynamically generated ones.

C. Scattering data

Elastic and inelastic total cross sections with K^-p in the initial state were measured in Refs. [20–24] (we did not take into consideration data from Ref. [25] with huge error bars). It is interesting that there are no comments about nonexistence of the total elastic cross sections (except Refs. [1] and [2]) due to the singularity of the pure Coulomb transition matrix T_{ba}^c in (2), while the "total elastic" cross sections are plotted by almost every author of $\bar{K}N$ interaction models. Having Coulomb interaction directly included into the calculations, we could not ignore the problem. We defined the "total elastic" K^-p cross section following the experimental works [20,25] as the differential cross section integrated over the region $-1 \leqslant \cos\theta \leqslant 0.966$ instead of $-1 \leqslant \cos\theta \leqslant 1$.

D. Threshold branching ratios

Three threshold branching ratios of K^-p scattering were measured rather accurately [26,27]. One of them is

$$\gamma = \frac{\Gamma(K^-p \to \pi^+\Sigma^-)}{\Gamma(K^-p \to \pi^-\Sigma^+)} = 2.36 \pm 0.04. \tag{16}$$

We oriented on the medium value

$$\gamma = 2.36. \tag{17}$$

The other two ratios R_c and R_n, containing $K^-p \to \pi^0\Lambda$ cross sections,

$$R_c = \frac{\Gamma(K^-p \to \pi^+\Sigma^-, \pi^-\Sigma^+)}{\Gamma(K^-p \to \text{all inelastic channels})} = 0.664 \pm 0.011, \tag{18}$$

$$R_n = \frac{\Gamma(K^-p \to \pi^0\Lambda)}{\Gamma(K^-p \to \text{neutral states})} = 0.189 \pm 0.015, \tag{19}$$

could not be used in a straightforward way because we did not include the $\pi^0\Lambda$ channel directly into our calculations. However, the effect of the channel was effectively taken into account by allowing the $\lambda^1_{\bar{K}N,\bar{K}N}$ parameter to have nonzero imaginary part (it significantly improved the agreement with the experimental cross sections). It is easy to find from the measured K^-p threshold branching ratios γ, R_c, and R_n that the relative weight of the $\pi^0\Lambda$ channel at K^-p threshold among all possible inelastic channels is approximately equal to 6%. So, the introduced imaginary part only slightly breaks unitarity, in contrast to what happens when a one-channel complex $\bar{K}N$ potential is used, approximately accounting for the main inelastic $\pi\Sigma$ channel.

From existing R_c and R_n we constructed a new threshold branching ratio

$$R_{\pi\Sigma} = \frac{\Gamma(K^- p \to \pi^+\Sigma^-) + \Gamma(K^- p \to \pi^-\Sigma^+)}{\Gamma(K^- p \to \pi^+\Sigma^-) + \Gamma(K^- p \to \pi^-\Sigma^+) + \Gamma(K^- p \to \pi^0\Sigma^0)}. \tag{20}$$

From definitions of R_c and R_n [Eqs. (18) and (19)] using experimental data we obtained for the $R_{\pi\Sigma}$ an "experimental" value

$$R_{\pi\Sigma} = \frac{R_c}{1 - R_n(1 - R_c)} = 0.709 \pm 0.011. \tag{21}$$

We tried to reproduce the medium value

$$R_{\pi\Sigma} = 0.709. \tag{22}$$

The formulas (A20) and (A21) allow us to find parameters $\lambda_{\mathbb{I}_i,\mathbb{I}_j}$, $\beta_{\mathbb{I}_i}$ (and s) of our potentials in both one-pole and two-pole cases, which reproduce these experimental quantities. All our parameters, except $\lambda^1_{\bar{K}N,\bar{K}N}$, are real.

IV. RESULTS AND DISCUSSION

We started the calculations with inclusion of the Coulomb interaction and using physical masses in both $\bar{K}N$ and $\pi\Sigma$ channels. In Fig. 1 we show the role of the two isospin breaking effects (Coulomb interaction and physical masses using) separately in $\bar{K}N$ and $\pi\Sigma$ channels on the example of some cross sections. The isospin-conserving strong interaction is the same for all cases; the one-pole $\Lambda(1405)$ form version of the potential was used. It can be seen that while the inclusion of these effects in $\bar{K}N$ changes both the elastic and inelastic cross-sections considerably, especially in the low-energy region, they have practically no influence on the cross sections, being included in the $\pi\Sigma$ sector [four lines in the $K^- p \to \pi^-\Sigma^+$ (effects in $\pi\Sigma$) are almost indistinguishable, the same property have all other cross sections with $K^- p$ in the initial state]. This is understandable, since both corrections are important close to the corresponding thresholds, and the energy region of our interest lies close to $\bar{K}N$ threshold(s) (one or two) and far from $\pi\Sigma$ thresholds. Due to this we kept the Coulomb potential in $K^- p$ subsystem and physical

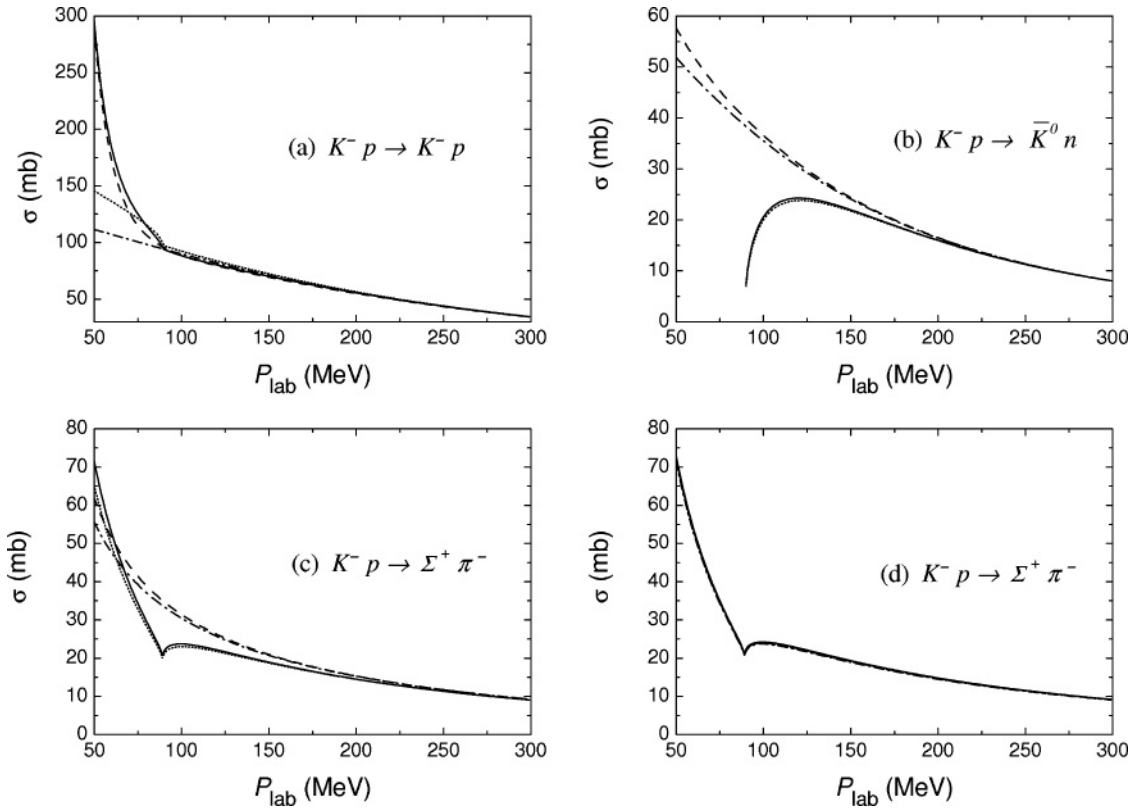

FIG. 1. Demonstration of isospin-breaking effects included in $\bar{K}N$ [plots (a)–(c)] and $\pi\Sigma$ [plot (d)] channels on several cross sections: Coulomb interaction and physical masses using are switched on (solid line), Coulomb is switched on and masses are switched off (dashed), Coulomb is off and masses are on (dotted), and Coulomb and masses are off (dashed-dotted) for the corresponding channel. The one-pole version of $\Lambda(1405)$ was used.

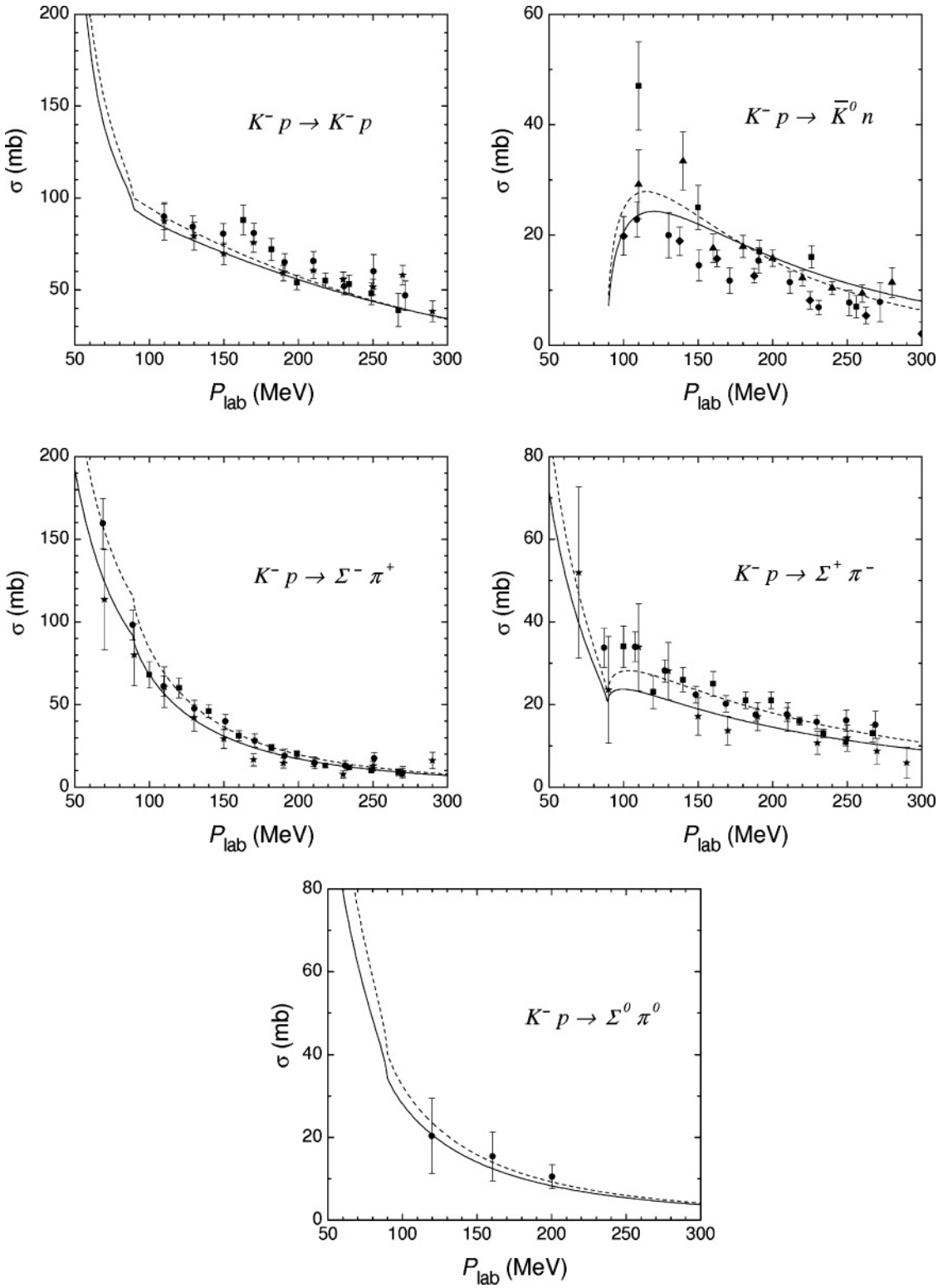

FIG. 2. Comparison of the obtained theoretical cross sections obtained with one-pole $\Lambda(1405)$ (solid line) and two-pole $\Lambda(1405)$ resonance form (dashed line) with experimental data [20–24].

masses in $\bar{K}N_{I=0}$, $\bar{K}N_{I=1}(K^-p, \bar{K}^0n)$ channels, while in $\pi\Sigma$ channels we used isospin averaged masses without the Coulomb interaction.

In the case of averaged masses without Coulomb in $\pi\Sigma$ the $\pi\Sigma_{I=2}(\mathbb{I}_5)$ channel is dynamically decoupled from the other four channels. So, we can work in particle space of four dimensions, corresponding to $\bar{K}N_{I=0}$, $\bar{K}N_{I=1}$ (or K^-p, $\bar{K}^0n$), $\pi\Sigma_{I=0}$, and $\pi\Sigma_{I=1}$ channels.

We succeeded in obtaining parameters of the potentials with one- and two-pole $\Lambda(1405)$ structure. The best set of the obtained parameters for the one-pole $\Lambda(1405)$ is:

$$\begin{aligned}\beta_{\bar{K}N}^{\text{1pole}} &= 3.4\ \text{fm}^{-1}\\ \beta_{\pi\Sigma}^{\text{1pole}} &= 1.9\ \text{fm}^{-1}\\ \underline{\underline{\Lambda}}^{\text{1pole}}(\mathbb{I}) &= \begin{pmatrix} -1.31 & 0 & 0.62 & 0\\ 0 & 1.76-i0.24 & 0 & 1.90\\ 0.62 & 0 & 0.18 & 0\\ 0 & 1.90 & 0 & 1.24\end{pmatrix};\end{aligned} \tag{23}$$

for the two-pole $\Lambda(1405)$ it is:

$$\begin{aligned}\beta_{\bar{K}N}^{\text{2pole}} &= 3.2\ \text{fm}^{-1}\\ \beta_{\pi\Sigma}^{\text{2pole}} &= 1.0\ \text{fm}^{-1}\\ s &= -0.87\\ \underline{\underline{\Lambda}}^{\text{2pole}}(\mathbb{I}) &= \begin{pmatrix} -1.06 & 0 & 0.40 & 0\\ 0 & 0.97-i0.11 & 0 & 1.13\\ 0.40 & 0 & -0.01 & 0\\ 0 & 1.13 & 0 & 0.61\end{pmatrix}.\end{aligned} \tag{24}$$

Here we assumed isospin independence of the range parameters:

$$\beta_{\mathbb{I}_1} = \beta_{\mathbb{I}_2} \equiv \beta_{\bar{K}N}, \tag{25}$$

$$\beta_{\mathbb{I}_3} = \beta_{\mathbb{I}_4} \equiv \beta_{\pi\Sigma}. \tag{26}$$

Our results for the cross sections with best set of the obtained parameters with one-pole and two-pole $\Lambda(1405)$ are presented in Fig. 2: the elastic $K^-p \to K^-p$ cross section and inelastic $K^-p \to \bar{K}^0n$, $K^-p \to \pi^+\Sigma^-$, $K^-p \to \pi^-\Sigma^+$, and $K^-p \to \pi^0\Sigma^0$ cross sections are compared with existing experimental data [20–24]. It shows that both versions of the potential are equally good in describing the experimental data within the experimental errors. Due to this fact, unfortunately, it is not possible to give preference to one of the $\Lambda(1405)$ versions.

Other physical characteristics of the obtained one-pole and two-pole potentials are shown in Table I: pole positions z_1 and z_2 (obviously, z_2 exists in a two-pole variant of the potential only), $1s$ kaonic hydrogen level shift ΔE_{1s}, and width Γ_{1s}. Threshold branching ratios γ (17) and $R_{\pi\Sigma}$ (22) are reproduced exactly in both cases. Having a complete set of potential parameters makes it possible to calculate the strong K^-p scattering length corresponding to the given ΔE_{1s} and Γ_{1s} exactly. The a_{K^-p} for both potentials are also shown in Table I.

The first pole positions z_1 for both versions of the potential have close real parts and the same imaginary ones, however, all three numbers differ from the PDG data for mass and width of $\Lambda(1405)$ resonance (10). The characteristics of the two poles

TABLE I. Physical characteristics of the obtained one-pole and two-pole potentials: pole positions z_1 and z_2, level shift ΔE_{1s} and width Γ_{1s} of kaonic hydrogen, and corresponding exact strong scattering length a_{K^-p}. Threshold branching ratios (17) and (22) are reproduced exactly.

	One-pole $\Lambda(1405)$	Two-pole $\Lambda(1405)$
z_1 (MeV)	$1409 - i32$	$1412 - i32$
z_2 (MeV)	–	$1380 - i105$
ΔE_{1s} (eV)	-396	-407
Γ_{1s} (eV)	370	476
a_{K^-p} (fm)	$-1.07 + i0.59$	$-1.08 + i0.76$

z_1 and z_2 in the two-pole $\Lambda(1405)$ version are the same as in Ref. [6]: one of them has less mass and larger width, while the other is heavier with narrower width. However, the positions of z_1 and z_2 differ from those in Ref. [6].

We also plotted the pole trajectories when the nondiagonal elements of the Λ of Eq. (A18), connecting the $\bar{K}N$ and $\pi\Sigma$ channels, were gradually reduced to zero from their original values; see Fig. 3. Other constants of the potentials remained unchanged. The figure shows that for both potential versions the higher-lying poles move to the real axis, providing real bound states with surprisingly small binding energies of 1–2 MeV. These limiting binding energies are smaller than those found in Ref. [4]. The second pole for the two-pole version moves downward under the $\pi\Sigma$ threshold on an unphysical sheet.

It is not absolutely clear how to relate the obtained potentials to the shape of the $\Lambda(1405)$ resonance. The experimental shape of the resonance is deduced from missing mass experiments since direct $\pi\Sigma$ data are not available. However, their relation to the pole structure of the two-body T matrix is not trivial and needs further investigation. Examples of this interpretation ambiguity are shown in Fig. 4, where elastic $\pi\Sigma$ cross sections

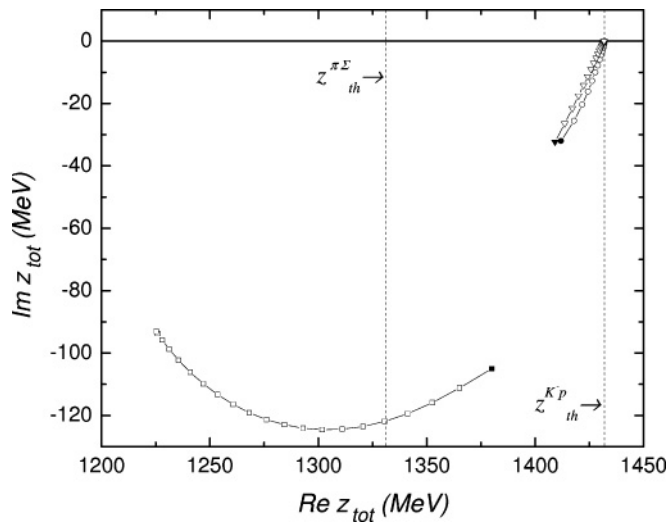

FIG. 3. Pole trajectories when the coupling between the $\bar{K}N$ and $\pi\Sigma$ channels is switched off for the one-pole $\Lambda(1405)$ variant (triangles) and the two-pole variant (circles and squares). The dark symbol denotes the original position of the corresponding pole.

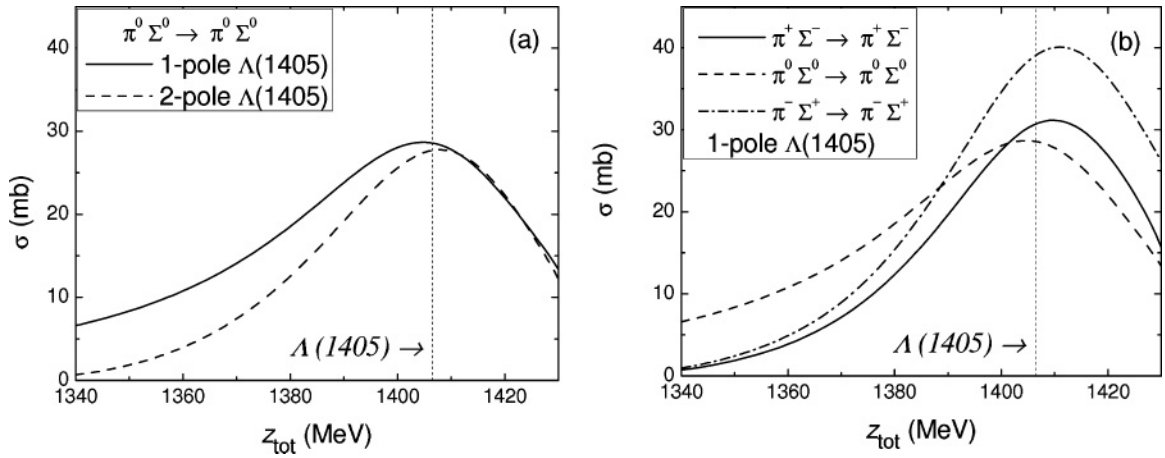

FIG. 4. The calculated $\pi\Sigma$ elastic cross sections in different charge channels: (a) $\pi^0\Sigma^0$ (proportional to purely $I = 0$) cross sections given by the one-pole and two-pole $\Lambda(1405)$ potentials and (b) three charge channel cross sections for the one-pole potential. The vertical line marks the medium PDG mass $M_\Lambda^{\rm PDG} = 1406.5$ MeV of the resonance [19].

in different charge channels are plotted. It can be seen that from the shapes of these curves it would be hard to deduce unambiguously the resonance parameters, given in Table I.

Another example is given in Fig. 5, where real and imaginary parts of the elastic K^-p amplitude for the two versions of the potential are depicted. At the the resonance positions real parts of $f_{K^-p\to K^-p}$ have zeros (situated at different, in respect to the medium PDG value, sides), while imaginary parts have their maxima (at slightly lower energies). The Coulomb singularities are seen almost at the K^-p threshold.

We plotted also the obtained parameters of kaonic hydrogen $(\Gamma_{1s}, |\Delta E_{1s}|)$, shown in Table I, together with the experimental 1σ regions of KEK and DEAR results; see Fig. 6. It is seen that obtained ΔE for the one-pole version is situated inside the KEK region, while for the two-pole variant it is slightly outside. Both values are close to each other, they definitely prefer the largest values of KEK $|\Delta E|$. All our attempts to move the shift values to the DEAR region led to drastic worsening of the agreement with the experimental cross sections. From this fact we do the same conclusion as did authors of Ref. [2]: the DEAR data on kaonic hydrogen measurements are inconsistent with the existing scattering data.

As for the widths, both are situated inside KEK 1σ limits, while the one-pole potential gives Γ_{1s} also inside DEAR, closely to its highest possible value. The important fact is that the obtained theoretical values of Γ_{1s} for the two versions of potentials differ largely. But, unfortunately, the accuracy

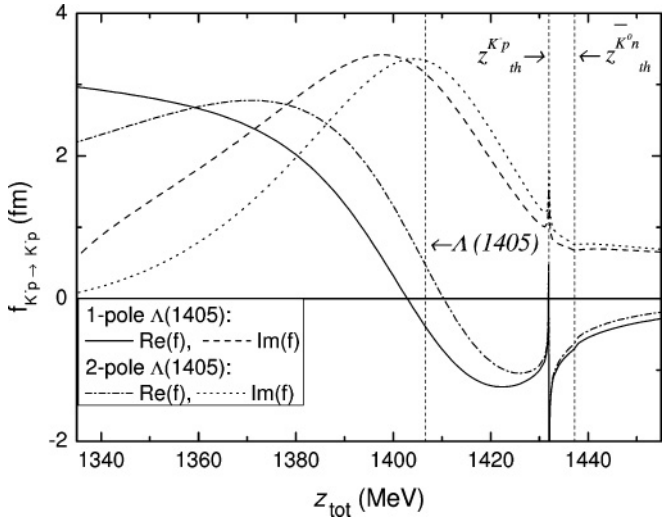

FIG. 5. Manifestation of $\Lambda(1405)$ resonance in $K^-p \to K^-p$ amplitude below the threshold for both versions of the potential. One-pole $\Lambda(1405)$: real (solid line) and imaginary (dashed line) parts of $f_{K^-p\to K^-p}$. Two-pole $\Lambda(1405)$: real (dash-dotted line) and imaginary (dotted line) parts of the amplitude. The vertical lines marks the medium PDG mass $M_\Lambda^{\rm PDG} = 1406.5$ MeV of the resonance [19], K^-p, and $\bar{K}^0n$ thresholds.

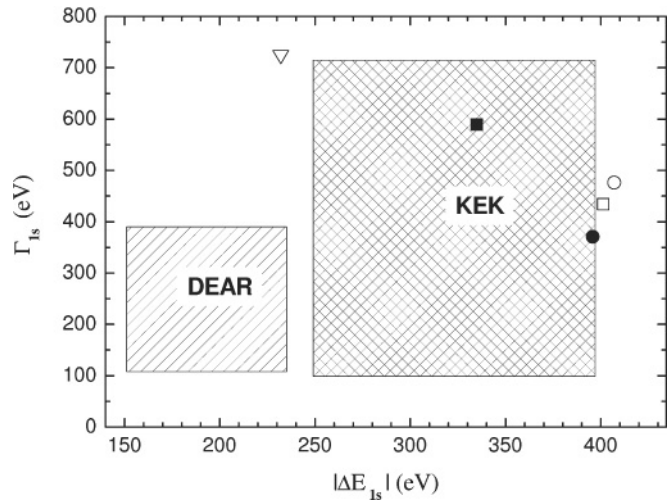

FIG. 6. DEAR and KEK 1σ confidence region of kaonic hydrogen $1s$ level shift $|\Delta E|$ (absolute value) and width Γ. The obtained theoretical results for the one-pole (solid circle) and two-pole (empty circle) variants of the potential are shown. The results of other theoretical models are also depicted: [1] (solid square), [2] (empty sqare), and [14] (empty triangle).

TABLE II. Isospin conserving $a^{\rm cons}$ (fm) and nonconserving $a^{\rm nonc}$ (fm) constituents of the total a (fm) K^-p scattering length for one-pole and two-pole versions of the potential.

	One-pole $\Lambda(1405)$	Two-pole $\Lambda(1405)$
$a^{\rm cons}_{K^-p}$	$-1.0561+i0.6977$	$-0.9949+i0.8648$
$a^{\rm nonc}_{K^-p}$	$0.0139+i0.1077$	$0.0851+i0.1048$
a_{K^-p}	$-1.07+i0.59$	$-1.08+i0.76$

of KEK results does not allow us to make a unique selection between them.

For comparison we plotted also the results of other theoretical models (Refs. [1,2], and [14]). The first two (Γ_{1s}, $|\Delta E_{1s}|$) values were obtained from the K^-p scattering lengths using corrected DT formula [13], while the last one was calculated directly. The chiral potential [2], aiming to reproduce mainly the K^-p scattering data, has a result (corresponding to the best a_{K^-p} value in the full approach) which is impressively close to ours, though the correctness of it is limited by the corrected DT formula accuracy. The previous potential of the same authors (version "u") has a different (Γ_{1s}, $|\Delta E_{1s}|$) value; however, it is also situated inside the 1σ KEK region. The result of Ref. [14] is far from all other theoretical values and outside both experimental regions. The reason could be their attempt to fit DEAR values simultaneously with the scattering data, which turned out to be unsuccessful. It is an additional demonstration of inconsistency of the DEAR results with the existing scattering data.

We see that both versions of our potential reproduce experimental cross sections equally well; by construction they exactly reproduce threshold branching ratios γ and $R_{\pi\Sigma}$. The obtained values of the kaonic hydrogen level shift ΔE_{1s} in both versions of $\Lambda(1405)$ resonance are close to each other. However, there is rather large, more than 100 eV, difference between the K^-p widths Γ_{1s}. Having in mind a forthcoming experiment, SIDDHARTA [28], we hope that the new experimental value will be close to one of our numbers, allowing one to make a conclusion about the structure of $\Lambda(1405)$ resonance.

The combined effect of the inclusion of the Coulomb interaction and using physical masses of the particles can be illustrated by showing the isospin conserving and nonconserving parts of the K^-p scattering length; see Table II. The constituents are defined as

$$a^{\rm cons}_{K^-p} \equiv \tfrac{1}{2}\left(a^{00}_{\bar{K}N} + a^{11}_{\bar{K}N}\right), \tag{27}$$

$$a^{\rm nonc}_{K^-p} \equiv a^{01}_{\bar{K}N} = a^{10}_{\bar{K}N}, \tag{28}$$

where $a^{II'}_{\bar{K}N}$ denotes the elastic strong (Coulomb is switched off) $\bar{K}N$ on-shell amplitude with initial (final) pair isospin $I'(I)$ at the K^-p threshold. The total scattering length, also shown in Table II, is

$$a_{K^-p} = a^{\rm cons}_{K^-p} - a^{\rm nonc}_{K^-p}. \tag{29}$$

It is seen that real parts of nonconserving scattering lengths change the final results only slightly, especially in the one-pole case, where $a^{\rm nonc}_{K^-p}$ is 1% of a_{K^-p} (it is 8% for the two-pole variant). In contrast, the imaginary parts change isospin conserving scattering lengths essentially, the share of isospin nonconserving part is 18% for the one-pole and 14% for the two-pole case. Thus, isospin breaking effects, taken into account in our calculations, are important, especially for the strong K^-p scattering length.

The differences of the exact K^-p level shifts and widths, obtained from our potentials, from results provided by approximate formulas are demonstrated in Table III. The approximate DT [11] and corrected DT [13] values for the shift and width were obtained using our exact scattering length given in Table I. It is seen that the DT formula [11] gives a very inaccurate result for both characteristics of kaonic atom: the absolute value of the level shift and the width are overestimated. The same result was obtained with several model one-channel complex $\bar{K}N$ potentials in Ref. [12]. The widely used corrected Deser formula [13] gives a rather accurate result for the shift but underestimates the width of $1s$ level by 9–10%.

To see another effect of isospin nonconservation, we calculated the norms of our resonant states, which are strictly speaking non-normalizable; however, a regularization procedure and a generalized norm can be defined for them (see Ref. [29] and references therein). In our multichannel case the

TABLE III. Kaonic hydrogen $1s$ level shift ΔE (eV) and width Γ (eV), corresponding to the obtained scattering length: exact (this work), derived from Deser-Trueman formula [11], and from corrected Deser formula [13].

	One-pole $\Lambda(1405)$	Two-pole $\Lambda(1405)$
$\Delta E^{\rm exact}_{1s}$	-396	-407
$\Gamma^{\rm exact}_{1s}$	370	476
$\Delta E^{\rm DT}_{1s}$ [11]	-441	-445
$\Gamma^{\rm DT}_{1s}$ [11]	486	626
$\Delta E^{\rm MRR}_{1s}$ [13]	-395	-411
$\Gamma^{\rm MRR}_{1s}$ [13]	338	434

TABLE IV. One-pole potential: norms $\mathcal{N}$ of the strong $z_1 = (1409.0 - i32.0)$ MeV and Coulomb $z_c = (1431.9 - i1.9 \times 10^{-4})$ MeV resonances.

	z_1	z_c
$\mathcal{N}_{(\bar{K}N)_{I=0}}$	$1.288 - i0.0792$	$0.500014 - i0.000013$
$\mathcal{N}_{(\bar{K}N)_{I=1}}$	$0.0008 - i0.0020$	$0.499986 + i0.000012$
$\mathcal{N}_{(\pi\Sigma)_{I=0}}$	$-0.2885 + i0.0810$	$\sim 10^{-7}$
$\mathcal{N}_{(\pi\Sigma)_{I=1}}$	$-0.0001 + i0.0002$	$\sim 10^{-7}$
$\mathcal{N}_0$	$0.9993 + i0.0018$	$0.500014 - i0.000012$
$\mathcal{N}_1$	$0.0007 - i0.0018$	$0.499986 + i0.000012$
$\mathcal{N}_{K^-p}$	$0.681 - i0.061$	$0.999994 + i2.8 \times 10^{-6}$
$\mathcal{N}_{\bar{K}^0n}$	$0.608 - i0.020$	$\sim 10^{-6}$
$\mathcal{N}_{\pi^-\Sigma^+}$	$-0.101 + i0.031$	$\sim 10^{-7}$
$\mathcal{N}_{\pi^0\Sigma^0}$	$-0.096 + i0.027$	$\sim 10^{-7}$
$\mathcal{N}_{\pi^+\Sigma^-}$	$-0.092 + i0.023$	$\sim 10^{-7}$

TABLE V. Two-pole potential: norms $\mathcal{N}$ of the strong $z_1 = (1411.9 - i32.0)$ MeV, $z_2 = (1380.0 - i105.0)$ MeV, and Coulomb $z_c = (1431.9 - i2.4 \times 10^{-4})$ MeV resonances.

	z_1	z_2	z_c
$\mathcal{N}_{(\bar{K}N)_{I=0}}$	$1.587 - i0.4101$	$-0.7302 + i0.5856$	$0.500016 - i0.000018$
$\mathcal{N}_{(\bar{K}N)_{I=1}}$	$0.0003 - i0.0037$	$0.0003 + i0.0004$	$0.499984 + i0.000017$
$\mathcal{N}_{(\pi\Sigma)_{I=0}}$	$-0.5872 + i0.4134$	$1.730 - i0.5859$	$\sim 10^{-6}$
$\mathcal{N}_{(\pi\Sigma)_{I=1}}$	$0.0002 + i0.0004$	$-0.0001 - i0.0001$	$\sim 10^{-7}$
$\mathcal{N}_0$	$0.999565 + i0.003251$	$0.999837 - i0.000330$	$0.500016 - i0.000017$
$\mathcal{N}_1$	$0.000435 - i0.003251$	$0.000163 + i0.000330$	$0.499984 + i0.000017$
$\mathcal{N}_{K^-p}$	$0.838 - i0.253$	$-0.367 + i0.312$	$0.999992 + i3.5 \times 10^{-6}$
$\mathcal{N}_{\bar{K}^0n}$	$0.749 - i0.160$	$-0.363 + i0.274$	$\sim 10^{-6}$
$\mathcal{N}_{\pi^-\Sigma^+}$	$-0.200 + i0.152$	$0.577 - i0.209$	$\sim 10^{-7}$
$\mathcal{N}_{\pi^0\Sigma^0}$	$-0.196 + i0.138$	$0.577 - i0.195$	$\sim 10^{-7}$
$\mathcal{N}_{\pi^+\Sigma^-}$	$-0.192 + i0.124$	$0.576 - i0.182$	$\sim 10^{-7}$

norm of a resonance wave function Ψ can be written as

$$\mathcal{N} = ||\Psi|| = \sum_i ||\Psi_{\mathbb{P}_i}|| = \sum_i ||\Psi_{\mathbb{I}_i}||, \tag{30}$$

where partial norms $\mathcal{N}_{\mathbb{P}_i}(\mathcal{N}_{\mathbb{I}_i})$ are

$$\mathcal{N}_{\mathbb{P}_i} \equiv ||\Psi_{\mathbb{P}_i}|| = \int \Psi^2_{\mathbb{P}_i}(\vec{k}) d\vec{k}. \tag{31}$$

Note the square in Eq. (31) instead of the modulus squared, due to which the norms are complex. The details of calculating these norms in momentum representation can be found in Ref. [29]. In spite of the fact that the unique physical interpretation of complex norms is not completely clear yet, the total wave function Ψ can be normalized as $\mathcal{N} = ||\Psi|| = 1$ and in this case the partial norms $\mathcal{N}_{\mathbb{P}_i}(\mathcal{N}_{\mathbb{I}_i})$ can serve as a measure of contribution of different particle channels to Ψ. The partial norms of our nuclear and Coulomb resonances in both $\mathbb{P}$ and $\mathbb{I}$ representations are shown in Tables IV and V.

We define the $I = 0$ and $I = 1$ norms as

$$\begin{aligned} \mathcal{N}_0 &\equiv \mathcal{N}_{(\bar{K}N)_{I=0}} + \mathcal{N}_{(\pi\Sigma)_{I=0}} \quad \text{and} \\ \mathcal{N}_1 &\equiv \mathcal{N}_{(\bar{K}N)_{I=1}} + \mathcal{N}_{(\pi\Sigma)_{I=1}}. \end{aligned} \tag{32}$$

From the tables it is seen that the nuclear resonances are predominantly in the $I = 0$ channel, as expected. The $I = 1$ admixture shows up in the fourth digit. It is also noteworthy that in the two-pole case one of the resonances seems to be composed mainly from the $\bar{K}N$ pair, while the other one is from the $\pi\Sigma$. As for the Coulomb level, again as supposed, it is essentially a K^-p state. The isospin mixing manifests itself as a small deviation of $\mathcal{N}_{K^-p}$ from unity [or $\mathcal{N}_{(\bar{K}N)_{I=0}}$ and $\mathcal{N}_{(\bar{K}N)_{I=1}}$ from 0.5]. We see that in contrast to the strong scattering length case, isospin breaking effects play a minor role for the resonance wave functions.

V. CONCLUSIONS

To conclude, we constructed a new phenomenological strong isospin-dependent $\bar{K}N$-$\pi\Sigma$ potential and investigated the role of isospin breaking effects, such as direct inclusion of the Coulomb interaction and using physical masses in the calculations. The effects turned out to be important for reproducing the $1s$ kaonic level shift and width and for obtaining the correct K^-p strong scattering length. We found two "best" sets of potential parameters for one-pole and two-pole structures of the $\Lambda(1405)$ resonance which describe all experimental data: the level shift and width of the kaonic hydrogen $1s$ level within the 1σ KEK confidence region, K^-p threshold branching ratios γ and $R_{\pi\Sigma}$, elastic and inelastic K^-p cross sections, and the $\Lambda(1405)$ resonance shape. Attempts to move the obtained $(\Gamma, \Delta E)$ values toward the DEAR 1σ region led to drastic worsening of K^-p cross sections, so we came to the same conclusions as those in Ref. [2] that DEAR results are inconsistent with K^-p scattering data.

Our one- and two-pole "best" sets of parameters are of the same quality in describing existing experimental data. The only significant difference between one- and two-pole variants of the potential is between the kaonic hydrogen widths Γ_{1s}. However, even 106 eV are not sufficient for making conclusions about structure of the $\Lambda(1405)$ resonance due to much larger experimental errors of the KEK measurement. More precise experimental data on the K^-p atom, for example, from the forthcoming SIDDHARTA experiment [28], could choose one of the variants of $\Lambda(1405)$ structure. More precise data on K^-p cross sections are also highly desirable.

The $\bar{K}N$-$\pi\Sigma$ T matrices corresponding to the obtained potentials are suitable and will be used in a new three-body coupled-channels Faddeev calculation.

ACKNOWLEDGMENT

The work was supported by the Czech GA AVCR Grant KJB100480801.

APPENDIX

The state vector $|\Psi\rangle$ is an element of both configuration and particle space. In particle space we can use either the particle

pair basis $\mathbb{P}$ with elements $|\mathbb{P}_i\rangle$, $i = 1 \ldots 5$:

$$[|\mathbb{P}_i\rangle] = \left(|K^- p\rangle, |\bar{K}^0 n\rangle, |\pi^- \Sigma^+\rangle, |\pi^0 \Sigma^0\rangle, |\pi^+ \Sigma^-\rangle\right) \quad \text{(A1)}$$

or, equivalently, the isospin basis $\mathbb{I}$ with $|\mathbb{I}_i\rangle$, $i = 1 \ldots 5$:

$$[|\mathbb{I}_i\rangle] = (|\bar{K} N\rangle_{I=0}, |\bar{K} N\rangle_{I=1}, |\pi \Sigma\rangle_{I=0}, |\pi \Sigma\rangle_{I=1}, |\pi \Sigma\rangle_{I=2}). \quad \text{(A2)}$$

Here I is a two-particle isospin. The two bases are connected by an orthogonal matrix composed of the corresponding Clebsch-Gordan coefficients:

$$|\mathbb{I}_i\rangle = \sum_j |\mathbb{P}_j\rangle \langle \mathbb{P}|\mathbb{I}\rangle_{ji} \quad \text{(A3)}$$

with

$$\langle \mathbb{P}|\mathbb{I}\rangle = \begin{pmatrix} -1/\sqrt{2} & 1/\sqrt{2} & 0 & 0 & 0 \\ 1/\sqrt{2} & 1/\sqrt{2} & 0 & 0 & 0 \\ 0 & 0 & 1/\sqrt{3} & -1/\sqrt{2} & 1/\sqrt{6} \\ 0 & 0 & -1/\sqrt{3} & 0 & \sqrt{2/3} \\ 0 & 0 & 1/\sqrt{3} & 1/\sqrt{2} & 1/\sqrt{6} \end{pmatrix},$$

$$\langle \mathbb{I}|\mathbb{P}\rangle = \langle \mathbb{P}|\mathbb{I}\rangle^{\mathrm{T}}. \quad \text{(A4)}$$

The projections

$$\langle \mathbb{P}_i|\Psi\rangle = \Psi_{\mathbb{P}_i} \quad \text{and} \quad \langle \mathbb{I}_i|\Psi\rangle = \Psi_{\mathbb{I}_i} \quad \text{(A5)}$$

are state vectors in "ordinary" space. We can define column vectors

$$\underline{\Psi}(\mathbb{P}) = \{\Psi_{\mathbb{P}_i}\} \quad \text{and} \quad \underline{\Psi}(\mathbb{I}) = \{\Psi_{\mathbb{I}_i}\}. \quad \text{(A6)}$$

Obviously

$$\Psi_{\mathbb{I}_i} = \sum_j \langle \mathbb{I}|\mathbb{P}\rangle_{ij} \Psi_{\mathbb{P}_j} \quad \text{or} \quad \underline{\Psi}(\mathbb{I}) = \langle \mathbb{I}|\mathbb{P}\rangle \underline{\Psi}(\mathbb{P}). \quad \text{(A7)}$$

Correspondingly, operators in this case are matrices in particle space with indices according to the chosen representation:

$$\underline{\underline{O}}(\mathbb{I}) = [O_{\mathbb{I}_i \mathbb{I}_j}] \quad \text{or} \quad \underline{\underline{O}}(\mathbb{P}) = [O_{\mathbb{P}_i \mathbb{P}_j}] \quad \text{(A8)}$$

and the matrix elements $O_{\mathbb{I}_i \mathbb{I}_j}(O_{\mathbb{P}_i \mathbb{P}_j})$ are operators in usual configuration space. Again

$$O_{\mathbb{I}_i \mathbb{I}_j} = \sum_{st} \langle \mathbb{I}|\mathbb{P}\rangle_{is} O_{\mathbb{P}_s \mathbb{P}_t} \langle \mathbb{P}|\mathbb{I}\rangle_{tj} \quad \text{or} \quad \underline{\underline{O}}(\mathbb{I}) = \langle \mathbb{I}|\mathbb{P}\rangle \, \underline{\underline{O}}(\mathbb{P}) \langle \mathbb{P}|\mathbb{I}\rangle. \quad \text{(A9)}$$

Here and in what follows the single and double underlining denotes vectors and matrices in particle space, respectively.

Our basic operators are H^0, V^c, and V^s, and [having in mind Eqs. (4)–(7)] $G^c(z)$. To define our multichannel problem, we have to specify these operators in particle space. The operators H^0, V^c, and $G^c(z)$ do not change the particle composition, therefore they can be conveniently defined in $\mathbb{P}$ representation, where they are diagonal. Thus

$$H^0(\mathbb{P})_{ij} = \delta_{\mathbb{P}_i, \mathbb{P}_j} H^0_{\mathbb{P}_i} = \delta_{\mathbb{P}_i, \mathbb{P}_j} \left(\frac{\hat{p}^2}{2\mu_{\mathbb{P}_i}} + E^{\mathrm{th}}_{\mathbb{P}_i} \right), \quad \text{(A10)}$$

where $\mu_{\mathbb{P}_i}$ and $E^{\mathrm{th}}_{\mathbb{P}_i}$ are the reduced mass and threshold energy for the particle pair $\mathbb{P}_i$, respectively, $\hat{p}$ is an operator of relative momentum. The Coulomb potential acts obviously only between charged particle pairs, therefore its matrix elements are

$$V^c(\mathbb{P})_{ij} = \delta_{\mathbb{P}_i, \mathbb{P}_j} V^c_{\mathbb{P}_i} \quad \text{(A11)}$$

with

$$V^c_{K^- p} = V^c_{\pi^- \Sigma^+} = V^c_{\pi^+ \Sigma^-} = v^c \quad \text{and} \quad V^c_{\bar{K}^0 n} = V^c_{\pi^0 \Sigma^0} = 0. \quad \text{(A12)}$$

Here $v^c = -e^2/r$ is an ordinary Coulomb potential between two particles with charges $+1$ and -1. Similarly, the corresponding Green's function matrix has the form

$$G^c(\mathbb{P})_{ij} = \delta_{\mathbb{P}_i, \mathbb{P}_j} G^c_{\mathbb{P}_i}(z) \quad \text{(A13)}$$

with

$$G^c_{\mathbb{P}_i}(z) = \left(z - H^0_{\mathbb{P}_i} - V^c_{\mathbb{P}_i}\right)^{-1}. \quad \text{(A14)}$$

The strong interaction V^s, responsible for the transitions between different particle channels, is supposed to conserve the two-particle isospin $I(\mathbb{I}_i)$, therefore it is convenient to define it in $\mathbb{I}$ representation. We have chosen a separable form:

$$V^s(\mathbb{I})_{ij} = \delta_{I(\mathbb{I}_i), I(\mathbb{I}_j)} |g_{\mathbb{I}_i}\rangle \lambda_{\mathbb{I}_i, \mathbb{I}_j} \langle g_{\mathbb{I}_j}|, \quad \text{(A15)}$$

which can be conveniently rewritten as

$$V^s(\mathbb{I}) = \underline{\underline{|g\rangle}} \, \underline{\underline{\Lambda}} \, \underline{\underline{\langle g|}} \quad \text{(A16)}$$

with

$$|g(\mathbb{I})\rangle_{ij} = \delta_{\mathbb{I}_i, \mathbb{I}_j} |g_{\mathbb{I}_i}\rangle \quad \text{(A17)}$$

and

$$\underline{\underline{\Lambda}}(\mathbb{I}) = \begin{pmatrix} \lambda^0_{\bar{K}N, \bar{K}N} & 0 & \lambda^0_{\bar{K}N, \pi\Sigma} & 0 & 0 \\ 0 & \lambda^1_{\bar{K}N, \bar{K}N} & 0 & \lambda^1_{\bar{K}N, \pi\Sigma} & 0 \\ \lambda^0_{\pi\Sigma, \bar{K}N} & 0 & \lambda^0_{\pi\Sigma, \pi\Sigma} & 0 & 0 \\ 0 & \lambda^1_{\pi\Sigma, \bar{K}N} & 0 & \lambda^1_{\pi\Sigma, \pi\Sigma} & 0 \\ 0 & 0 & 0 & 0 & \lambda^2_{\pi\Sigma, \pi\Sigma} \end{pmatrix} \quad \text{(A18)}$$

(here we moved $I(\mathbb{I}_i) = I(\mathbb{I}_j)$ indices of the matrix elements to the right-up positions for a convenience). To complete the description of the matrix-vector analog of Eqs. (3)–(7), the initial (final) states $|\Phi^c_b\rangle$ have to be specified. For a given initial (final) particle pair labeled by $\mathbb{P}_i$ the particle space vector can be conveniently defined in $\mathbb{P}$ representation:

$$\left|\Phi^c_{\mathbb{P}_i}(\mathbb{P})_j\right\rangle = \delta_{\mathbb{P}_i, \mathbb{P}_j} \left|\Phi^c_{\mathbb{P}_i}\right\rangle \quad \text{(A19)}$$

with $|\Phi^c_{\mathbb{P}_i}\rangle$ being an ordinary configuration space state vector (with the Coulomb interaction taken into account, if it exists for that pair).

Now all operators and states are defined, and we are in a position to write down the particle space matrix analog of Eq. (6):

$$T^{sc}_{ba} = \left\langle \underline{\Phi}^{c(-)}_b \middle| \underline{g} \right\rangle \left(\underline{\underline{\Lambda}}^{-1} - \underline{\underline{\langle g|}} \, \underline{\underline{G^c}}(E + i\varepsilon) \underline{\underline{|g\rangle}} \right)^{-1} \left\langle \underline{g} \middle| \underline{\Phi}^{c(+)}_a \right\rangle. \quad \text{(A20)}$$

In the described matrix formulation of the problem the position of the bound states and resonances instead of Eq. (7) is determined by

$$\mathrm{Det}(\underline{\underline{\Lambda}}^{-1} - \underline{\underline{\langle g|G^c(z)|g\rangle}}) = 0. \tag{A21}$$

However, for writing out Eq. (A20) and (A21) in components it is necessary to use the same representation ($\mathbb{I}$ or $\mathbb{P}$) for all vectors and matrices. Since we are interested in obtaining parameters of the strong interaction V^s which is given in $\mathbb{I}$, we performed our calculations in this representation and transformed vectors and matrices defined in $\mathbb{P}$ into $\mathbb{I}$, using formulas (A4), (A7), and (A9). As a nontrivial example, $\underline{\underline{G^c}}(\mathbb{I})$ is not a diagonal matrix as $\underline{\underline{G^c}}(\mathbb{P})$ is (A13) but has the form:

$$\underline{\underline{G^c}}(\mathbb{I}) = \begin{pmatrix} \underline{\underline{G^c_{\bar{K}N}}}(\mathbb{I}) & \begin{matrix} 0 & 0 & 0 \\ 0 & 0 & 0 \end{matrix} \\ \begin{matrix} 0 & 0 \\ 0 & 0 \\ 0 & 0 \end{matrix} & \underline{\underline{G^c_{\pi\Sigma}}}(\mathbb{I}) \end{pmatrix} \tag{A22}$$

with

$$\underline{\underline{G^c_{\bar{K}N}}}(\mathbb{I}) = \begin{bmatrix} \frac{1}{2}\left(G^c_{K^-p} + G^c_{\bar{K}^0n}\right) & -\frac{1}{2}\left(G^c_{K^-p} - G^c_{\bar{K}^0n}\right) \\ -\frac{1}{2}\left(G^c_{K^-p} - G^c_{\bar{K}^0n}\right) & \frac{1}{2}\left(G^c_{K^-p} + G^c_{\bar{K}^0n}\right) \end{bmatrix} \tag{A23}$$

and

$$\underline{\underline{G^c_{\pi\Sigma}}}(\mathbb{I}) = \begin{bmatrix} \frac{1}{3}\left(G^c_{\pi^-\Sigma^+} + G^c_{\pi^0\Sigma^0} + G^c_{\pi^+\Sigma^-}\right) & -\frac{1}{\sqrt{6}}\left(G^c_{\pi^-\Sigma^+} - G^c_{\pi^+\Sigma^-}\right) & \frac{1}{3\sqrt{2}}\left(G^c_{\pi^-\Sigma^+} - 2G^c_{\pi^0\Sigma^0} + G^c_{\pi^+\Sigma^-}\right) \\ -\frac{1}{\sqrt{6}}\left(G^c_{\pi^-\Sigma^+} - G^c_{\pi^+\Sigma^-}\right) & \frac{1}{2}\left(G^c_{\pi^-\Sigma^+} + G^c_{\pi^+\Sigma^-}\right) & -\frac{1}{2\sqrt{3}}\left(G^c_{\pi^-\Sigma^+} - G^c_{\pi^+\Sigma^-}\right) \\ \frac{1}{3\sqrt{2}}\left(G^c_{\pi^-\Sigma^+} - 2G^c_{\pi^0\Sigma^0} + G^c_{\pi^+\Sigma^-}\right) & -\frac{1}{2\sqrt{3}}\left(G^c_{\pi^-\Sigma^+} - G^c_{\pi^+\Sigma^-}\right) & \frac{1}{6}\left(G^c_{\pi^-\Sigma^+} + 4G^c_{\pi^0\Sigma^0} + G^c_{\pi^+\Sigma^-}\right) \end{bmatrix} \tag{A24}$$

It can be seen that $\underline{\underline{G^c}}(\mathbb{I})$ has matrix elements connecting states with unequal isospins. They are proportional to difference of $\underline{\underline{G^c}}$ components in dissimilar particle pair channels $\mathbb{P}_i$. This isospin nonconservation has two independent sources. First, G^c of charged particles differs from $G^c = G^0$ of neutral pairs, and, second, due to the mass difference of the isomultiplet members, the particle pairs $\mathbb{P}_i$ have different reduced masses and threshold energies and, thus, according to Eq. (A10), different H^0-s and G^0-s. Neglecting these two effects in the $\pi\Sigma$ sector leads to a diagonal submatrix $\underline{\underline{G^c_{\pi\Sigma}}}(\mathbb{I})$.

[1] B. Borasoy, R. Nißler, and W. Weise, Phys. Rev. Lett. **94**, 213401 (2005); Eur. Phys. J. A **25**, 79 (2005).
[2] B. Borasoy, U.-G. Meißner, and R. Nißler, Phys. Rev. C **74**, 055201 (2006).
[3] Y. Akaishi and T. Yamazaki, Phys. Rev. C **65**, 044005 (2002); T. Yamazaki and Y. Akaishi, Phys. Lett. **B535**, 70 (2002).
[4] T. Hyodo and W. Weise, Phys. Rev. C **77**, 035204 (2008).
[5] J. A. Oller and U.-G. Meißner, Phys. Lett. **B500**, 263 (2001); D. Jido *et al.*, Nucl. Phys. **A725**, 181 (2003).
[6] V. K. Magas, E. Oset, and A. Ramos, Phys. Rev. Lett. **95**, 052301 (2005).
[7] I. Zychor *et al.*, Phys. Lett. **B660**, 167 (2008).
[8] L. S. Geng and E. Oset, Eur. Phys. J. A **34**, 405 (2007).
[9] M. Iwasaki *et al.*, Phys. Rev. Lett. **78**, 3067 (1997); T. M. Ito *et al.*, Phys. Rev. C **58**, 2366 (1998).
[10] G. Beer *et al.*, Phys. Rev. Lett. **94**, 212302 (2005).
[11] S. Deser *et al.*, Phys. Rev. **96**, 774 (1954); T. L. Trueman, Nucl. Phys. **26**, 57 (1961).
[12] J. Révai and N. V. Shevchenko, Few-Body Syst. **42**, 83 (2008).
[13] U.-G. Meißner, U. Raha, and A. Rusetsky, Eur. Phys. J. C **35**, 349 (2004).
[14] A. Cieplý and J. Smejkal, Eur. Phys. J. A **34**, 237 (2007).
[15] N. V. Shevchenko and J. Révai, Few-Body Syst. **44**, 187 (2008).
[16] Z. Bajzer, Z. Phys. A: Hadrons Nucl. **278**, 97 (1976).
[17] A. Deloff and J. Law, Phys. Rev. C **21**, 2048 (1980).
[18] W. Schweiger, W. Plessas, L. P. Kok, and H. van Haeringen, Phys. Rev. C **27**, 515 (1983).
[19] C. Amsler *et al.* (Particle Data Group), Phys. Lett. **B667**, 1 (2008).
[20] M. Sakitt *et al.*, Phys. Rev. **139**, B719 (1965).
[21] J. K. Kim, Phys. Rev. Lett. **14**, 29 (1965); Columbia University Report, Nevis, 149 (1966); Phys. Rev. Lett. **19**, 1074 (1967).
[22] W. Kittel, G. Otter, and I. Wacek, Phys. Lett. **21**, 349 (1966).
[23] J. Ciborowski *et al.*, J. Phys. G **8**, 13 (1982).
[24] D. Evans *et al.*, J. Phys. G **9**, 885 (1983).
[25] W. E. Humphrey and R. R. Ross, Phys. Rev. **127**, 1305 (1962).
[26] D. N. Tovee *et al.*, Nucl. Phys. **B33**, 493 (1971).
[27] R. J. Nowak *et al.*, Nucl. Phys. **B139**, 61 (1978).
[28] M. Cargnelli (SIDDHARTA Collaboration), Acta Phys. Slov. **55**, 7 (2005).
[29] E. Hernández and A. Mondragón, Phys. Rev. C **29**, 722 (1984).